ELSEVIER

Journal of Nuclear Materials 279 (2000) 189–200

journal of nuclear materials

www.elsevier.nl/locate/jnucmat

Microchemistry characterization by Auger electron spectroscopy of a cold-worked AISI-304L stainless steel

M. Hernández-Mayoral *, G. de Diego, M. García-Mazarío

CIEMAT, Avenida Complutense, 22, 28040 Madrid, Spain

Received 21 December 1998; accepted 19 January 2000

Abstract

Auger electron spectroscopy (AES) has been performed on grain boundaries of an AISI-304L stainless steel. The aim of the work was to study microchemistry at grain boundaries by AES after simulating irradiation effects by cold work followed by heat treatments. The results show that phosphorus was present at interfaces in all material conditions. Sometimes, phosphorus was accompanied by molybdenum and by chromium enrichment. Those analyses were attributed to ferrite/austenite interfaces while those where phosphorus was found alone were thought to belong to austenite/austenite interfaces. Cold work when combined with heat treatment at low temperature was shown to affect phosphorus and chromium segregation in a similar way to radiation-induced segregation. In this respect, cold work enhanced non-equilibrium phosphorus segregation to interfaces, while it induced chromium diffusion away from grain boundaries. Finally, corrosion and stress corrosion tests were performed to study the influence of this particular microchemistry on 304L performance.

1. Introduction

Intergranular cracking has been observed after extended neutron radiation exposure in some internal components of light water reactors made of austenitic stainless steels and nickel-based alloys [1]. The degradation process accelerated by the presence of irradiation has been called Irradiation Assisted Stress Corrosion Cracking (IASCC). When looking for the causes of the problem, the fact that a threshold of irradiation dose is needed for the failure suggests that the observed behaviour is strongly related with radiation-induced changes on microstructure or interface microchemistry [2]. Both microscopical aspects, microstructure and microchemistry, are believed to influence macroscopical properties of a material, and consequently they affect material behaviour under particular circumstances, as are those inside a nuclear reactor core. Independently of the cause of microscopic changes (radiation, cold work or thermal treatments) the reason why a particular microstructure or microchemistry affects material behaviour is not known.

Difficulties in handling irradiated material induce one to try a simulation of neutron irradiation effects by other means as, for example, irradiation with other particles, cold work, thermal treatments, etc. In the present study, changes in microchemistry at interfaces have been promoted in a 304L austenitic stainless steel by processes that simulate those that take place in materials during neutron irradiation. With that purpose, the material was cold worked to increase hardness and yield strength, and segregation was induced applying different heat treatments after cold work. In addition, two tests were performed to assess the susceptibility of this steel, with its particular microstructure and microchemistry, to corrosion and stress corrosion cracking.

Microchemistry was characterised by Auger electron spectroscopy (AES). The most commonly used techniques to characterize grain boundary microchemistry are energy dispersive X-ray analysis in transmission electron microscopy (TEM/EDS) and AES, although they have disadvantages as well as advantages. Some of

* Corresponding author. Tel.: +34-91 346 6618; fax: 34-91 346 6661.

E-mail address: m.mayoral@ciemat.es (M. Hernández-Mayoral).

0022-3115/00/$ - see front matter
PII: S0022-3115(00)00011-8

the problems in grain boundary microchemistry studies by means of AES are the need to obtain intergranular fracture and that results can be influenced by the presence of grain boundary precipitation. However, if intergranular fracture is achieved, AES is a suitable technique to analyse impurities with a narrow segregation profile. Using TEM/EDS, grain boundary analysis can be performed avoiding grain boundary precipitation. However, TEM/EDS analysis is limited to those boundary planes that can be accurately oriented parallel to the incident electron beam direction and each thin foil may yield only a few grain boundaries.

2. Experimental

2.1. Material

The material under study was an AISI-304L with 0.02 wt% of carbon content. Its composition is shown in Table 1.

The material was studied in the as-received condition (non-cold-worked, named A condition) followed by three different heat treatments, 500°C for 100 and 1000 h and 400°C, 1000 h, named 1, 2 and 3, respectively. The rest of the conditions studied were: this material with two degrees of cold work: 10% and 30% (B and C conditions, respectively), and also followed by three heat treatments as before. Temperature of heat treatments was chosen low enough in order to avoid the loss of changes produced by cold work. The set of conditions studied are summarized in Table 2. From now on, the names given to every condition in Table 2 will be used in the text.

Microstructural characterization was performed by metallography in all the conditions referred in Table 2.

2.2. Auger spectroscopy analyses

Microchemistry at interfaces was studied using a PHI 660 scanning Auger electron spectroscope. Two notched samples per condition were studied, which were fractured inside the Auger vacuum chamber. In order to promote intergranular fracture, samples were cathodically charged with hydrogen as follows. First at all, samples were electropolished in 60% phosphoric acid and 40% sulphuric acid. Then, they were cathodically charged with hydrogen in a 0.1 N sulphuric acid with arsenic in the form of As_2O_3 as a hydrogen recombination poison, at a solution temperature of 70°C. After a period of charge of 72 h, the samples were taken out from the cathodic charge, and immediately loaded into the AES vacuum chamber. Samples were fractured in situ by tension at a deformation rate of 1 μm/s, at a pressure of 10^{-9} Torr, with a specially designed fracture stage attached to the spectrometer that allows to keep on and to analyze the two halves resulting from the fracture. Once the fracture was achieved, a secondary electron image of the fracture surface was obtained to identify the areas of the sample that failed intergranularly. Analyses in spots of about 100 nm of diameter (and ~3 nm in depth) were performed on grain boundary facets and on the ductile fracture for comparison. The acceleration voltage of the primary electron beam was 10 kV and an Auger spectrum from 25 to 1025 eV was recorded from every point analysed, where it was possible to identify the elements present on the fracture surface. Results are reported as atomic concentration, calculated following Davis et al. [3]. Sensitivity factors of iron, chromium and nickel have been obtained comparing calculated concentration at the ductile areas to the composition of the material. Therefore, 0.200, 0.280, 0.220, have been used for iron, chromium and nickel, respectively. Sensitivity factors for the rest of the elements were taken from the above reference.

2.3. Corrosion tests

The corrosion behaviour was examined in boiling 5N HNO_3 + 0.46N $K_2Cr_2O_7$. This solution provides a highly aggressive environment and is widely used to detect susceptibility to intergranular corrosion of a non-sensitized material due to grain boundary impurities [4–6]. Five samples per condition were tested for four periods, each of 6 h, with a fresh dissolution in every

Table 1
Composition of AISI-304L material

	C	Fe	Cr	Ni	Mn	P	S	Mo	N	Si	Ti	Nb
304L	0.020	Bal.	18.5	8.31	1.67	0.026	0.003	0.39	0.069	0.49	<0.01	<0.01

Table 2
Summary of the different conditions studied by AES

A1 = 0%CW + 500°C, 100 h	B1 = 10%CW + 500°C, 100 h	C1 = 30%CW + 500°C, 100 h
A2 = 0%CW + 500°C, 1000 h	B2 = 10%CW + 500°C, 1000 h	C2 = 30%CW + 500°C, 1000 h
A3 = 0%CW + 400°C, 1000 h	B3 = 10%CW + 400°C, 1000 h	C3 = 30%CW + 400°C, 1000 h

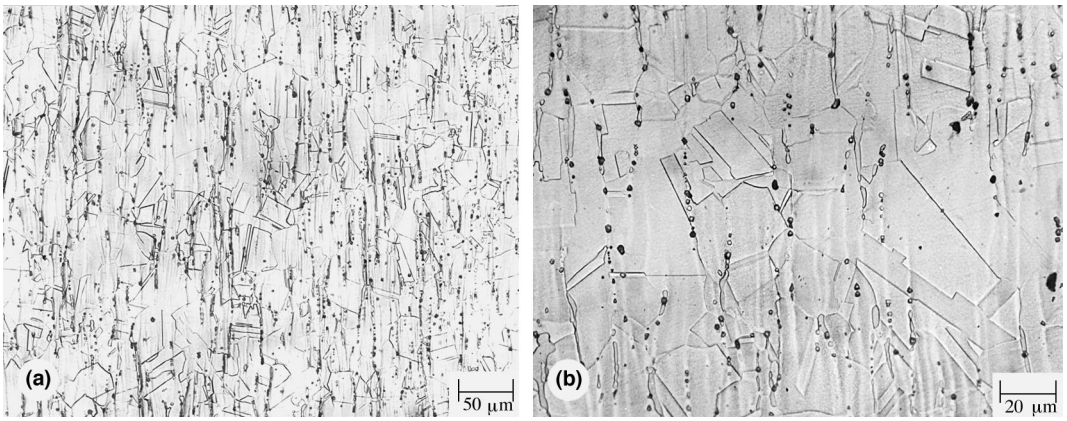

Fig. 1. Microstructure of non-cold-worked condition followed by a heat treatment at 500°C, 100 h (A1).

period. The total duration of the test was 24 h. Material susceptibility was determined by measuring weight loss per area and per unit of time.

Also, constant extension rate tests (CERT) were carried out in a refreshed autoclave. Operation conditions were similar to a boiling water reactor environment, 288°C and 80 kg/cm^2. Test were performed until the sample was broken in water with 200 ppb of oxygen content and a conductivity less than μs/cm, being the extension rate 5.6×10^{-7} s^{-1}. Every test was performed with six samples at the same time inside the autoclave.

3. Results

3.1. Microstructure

The material in the as-received condition showed an austenitic matrix with delta-ferrite oriented along a preferred direction. The volume fraction of delta-ferrite, estimated by magnetic measurements and using Schaeffler diagram, was between 1.5% and 5%, depending on the spatial direction considered. The material scarcely showed neither intergranular nor transgranular precipitates. The ASTM grain size was 7.5.

Microstructure of non-cold-worked conditions followed by heat treatment, named A1, A2 and A3 did not show great changes compared to the as-received condition. An example of this microstructure is shown in Fig. 1(a) and (b). When samples were cold worked and then heat-treated, their microstructure changed with respect to the as-received condition. Conditions with 10% of cold work and subsequent heat treatments, named B1, B2 and B3, showed slip bands due to deformation produced by cold work. This deformation induced the formation of martensite at the slip bands. Therefore, there were three different phases: an austenite matrix, some residual delta-ferrite and deformation-induced martensite associated to slip bands. All these conditions B presented groups of transgranular precipitates at deformation bands. This fact can be observed in Fig. 2(a)

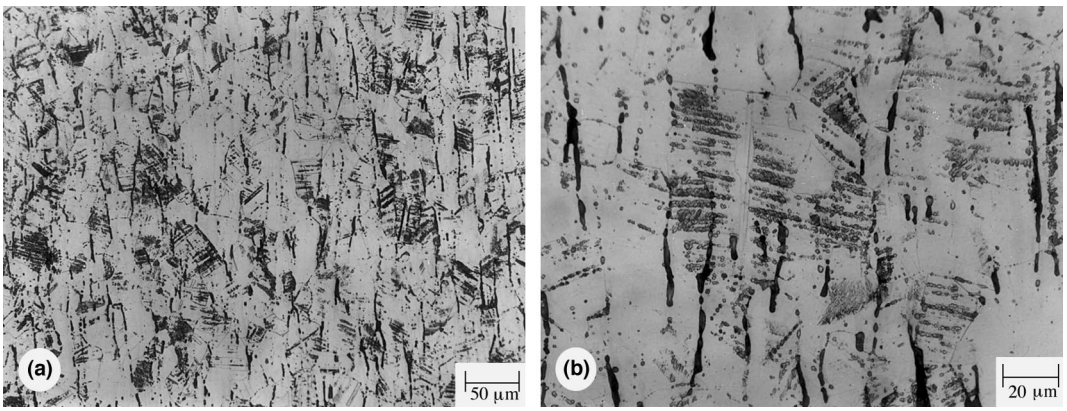

Fig. 2. Microstructure after 10% of cold work followed by a heat treatment at 500°C, 1000 h (B2).

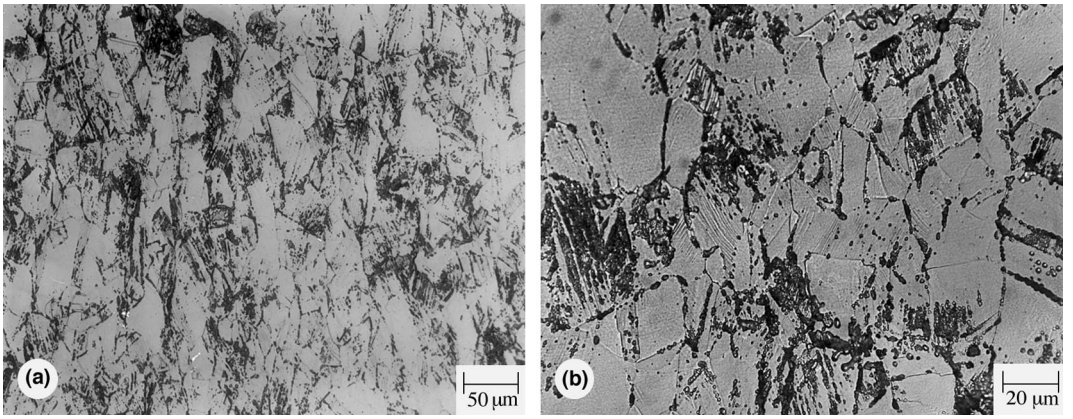

Fig. 3. Microstructure after 30% of cold work followed by a heat treatment at 500°C, 1000 h (C2).

Table 3
Precipitates and phase distribution

	Intergranular precipitates	Transgranular precipitates	Other phases
A1	–	–	δ-ferrite
A2	Slight	–	δ-ferrite
A3	–	–	δ-ferrite
B1	–	Medium	δ-ferrite + martensite
B2	Slight	High	δ-ferrite + martensite
B3	–	Slight	δ-ferrite + martensite
C1	–	Medium	δ-ferrite + martensite
C2	High	Very high	δ-ferrite + martensite
C3	–	Slight	δ-ferrite + martensite

and (b). Finally, conditions with 30% cold work followed by heat treatment, named C, showed a high increase in slip band density and deformation-induced martensite. Intergranular precipitation was only observed in condition C2 (500°C, 1000 h), together with a high transgranular precipitation. On the other hand, C1 (500°C, 100 h) and C3 (400°C, 1000 h), showed medium and slight transgranular precipitation, respectively. An example of this microstructure is shown in Fig. 3(a) and (b). Table 3 summarizes these results.

3.2. Auger analysis results

In all conditions, at least one out of two samples gave some degree of intergranular fracture, though the percentage of intergranular features was always quite low. Fig. 4 shows, as an example, an image of one of the fracture surfaces studied. Here, a preferred direction can be observed. That appearance is representative of fracture surfaces of all the conditions studied. It is worth noting that this feature appeared even in non-cold-worked specimens. That appearance is attributed to the presence of a second phase, the delta ferrite in the austenite matrix, oriented with a preferred direction and

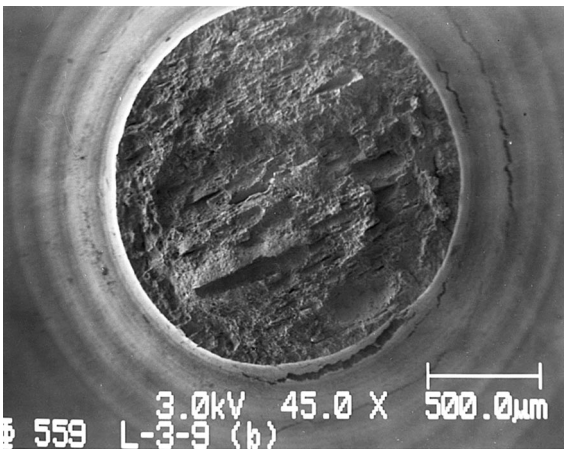

Fig. 4. SEM image of the fracture surface obtained in the Auger vaccum chamber. Sample with 30% of cold work followed by 500°C, 100 h, (C2).

that did not disappear with the heat treatment. In general, the fracture surfaces showed a ductile area in the inner part of the sample and an area of intergranular appearance at the edge of the fracture surface that can

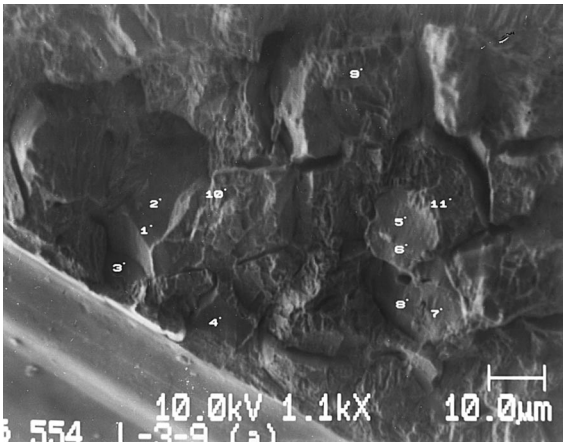

Fig. 5. SEM image of an area that showed some intergranular features. Sample with 30% of cold work followed by 500°C, 1000 h (C2).

be distinguished at higher magnification, as shown in Fig. 5.

Fig. 6(a)–(c) show, as an example, three typical Auger spectra obtained from a fracture surface. They correspond to analyses performed at ductile, Fig. 6(a), and at intergranular areas, Fig. 6(b) and (c). In the ductile area, the spectra show the presence of the main alloying elements, iron, chromium and nickel, and also the presence of carbon and oxygen. Spectra from intergranular areas show the same elements as in ductile areas and the presence of phosphorus, Fig. 6(b) and (c). Some of them also showed the presence of molybdenum, Fig. 6(c). Three conditions showed spectra of the first type only, similar to Fig. 6(b), that are non cold worked followed by 500°C, 1000 h, and 10% cold worked followed by 500°C, 1000 h and 400°C, 1000 h (A2, B2 and B3, respectively), while the rest of the conditions showed the two kinds of spectra on grain boundaries. It was observed that the percentage of analyses at intergranular areas with molybdenum is under 16% in all cases except conditions with 10% and 30% of cold work followed by 500°C, 100 h, (B1 and C1), where it is 46% and 33%, respectively. Clearly, two kinds of spectra are observed at intergranular areas being the main difference between them molybdenum presence or absence. Moreover, spectra with molybdenum always showed higher phosphorus and chromium peaks than spectra without molybdenum. Analyses without molybdenum were different among themselves as regards peak size of phosphorus, chromium and nickel. Both the two kinds of spectra and the difference in peak sizes result in a non-homogeneous distribution of phosphorus, chromium and molybdenum at interfaces. On the other hand, the two kinds of spectra together with observed microstructure suggest that analyses were performed on two different types of interfaces, those between ferrite and austenite phases, and those between austenite grain boundaries. Table 4 summarizes the qualitative observations from Auger spectra of all the conditions referred in Table 2, as well as the number of samples that showed intergranular fracture and the number of analyses on intergranular areas where the different observations were found.

Following the above qualitative descriptions, a quantitative study is presented. Average concentration was calculated for every element identified, both at the ductile and intergranular areas, for every condition. The average value was calculated by taking the whole number of analyses performed on all specimens. Those average values and their standard deviation, $\pm 1\sigma$, are summarized in Table 5.

Table 4
Summary of Auger results

Material condition	Samples with IG/ No. total samples	Observations	No. analyses/No. total IG analyses
A1	1/2	Low P, Cr $\gtrsim$ matrix, no Mo, Ni ~ matrix	11/13 (85%)
		High P, Cr $\gg$ matrix, Mo, Ni ~ matrix	2/13 (15%)
A2	1/2	High P, Cr > matrix, no Mo, Ni ~ matrix	8/8 (100%)
A3	2/2	Low P, Cr $\gtrsim$ matrix, no Mo, Ni ~ matrix	26/31 (84%)
		High P, Cr $\gg$ matrix, Mo, Ni ~ matrix	5/31 (16%)
B1	1/2	Low P, Cr $\gtrsim$ matrix, no Mo, Ni < matrix	14/26 (54%)
		High P, Cr > matrix, Mo, Ni < matrix	12/26 (46%)
B2	2/2	High P, Cr ~ matrix, no Mo, Ni $\gtrsim$ matrix	42/42 (100%)
B3	1/2	Low P, Cr $\gtrsim$ matrix, no Mo, Ni ~ matrix	4/4 (100%)
C1	1/2	Low P, Cr $\gtrsim$ matrix, no Mo, Ni $\gtrsim$ matrix	14/21 (67%)
		High P, Cr > matrix, Mo, Ni ~ matrix	7/21 (33%)
C2	2/2	High P, Cr ~ matrix, no Mo, Ni > matrix	31/33 (94%)
		High P, Cr > matrix, Mo, Ni ~ matrix	2/33 (6%)
C3	1/2	Low P, Cr $\gtrsim$ matrix, no Mo, Ni > matrix	21/24 (88%)
		High P, Cr > matrix, Mo, Ni > matrix	3/24 (12%)

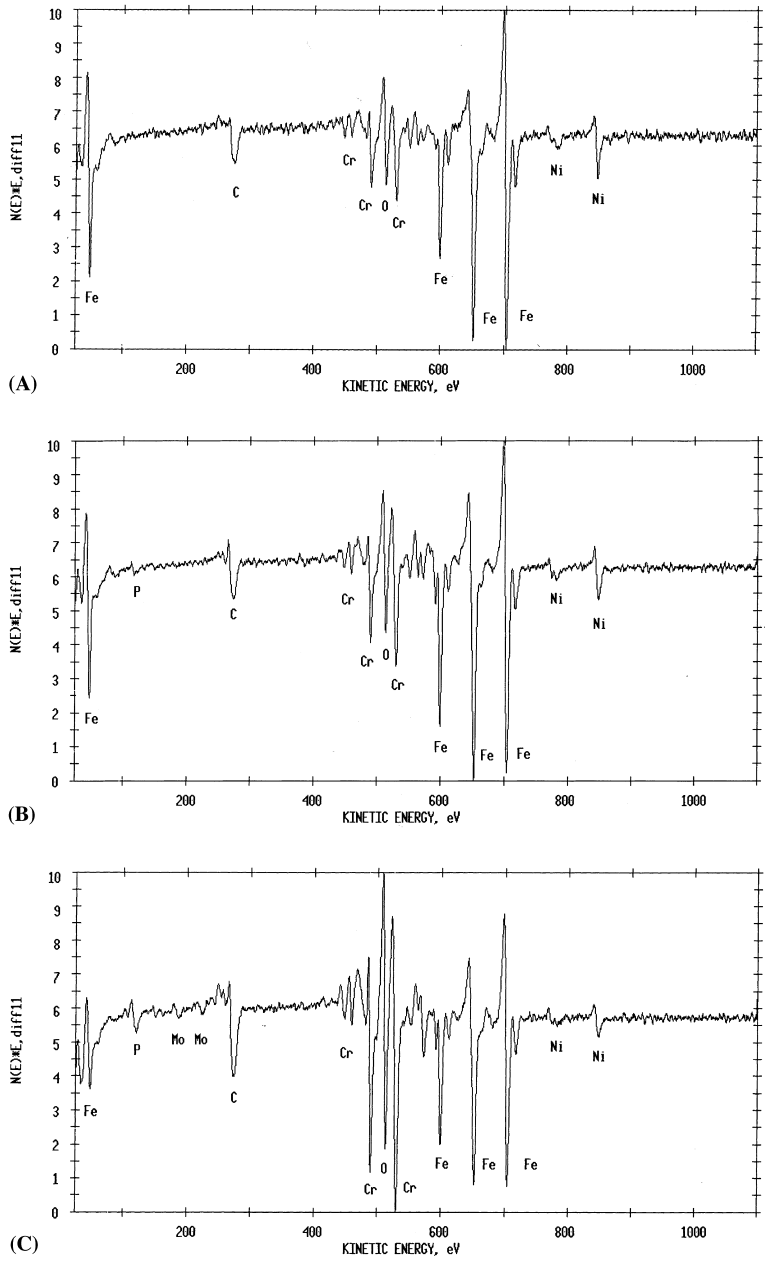

Fig. 6. Auger spectra obtained from (a) ductile area and (b) and (c) intergranular areas.

Composition characterization at interfaces shows the same microchemistry in conditions non cold worked followed by heat treatment, named A. That microchemistry consisted of phosphorus and chromium enrichment at interfaces with 1.8% and 23%, respectively. In general, chromium concentration at grain boundaries presented a high standard deviation in data, showing the big scatter in concentration analysis at different areas in the same sample, where sometimes a 30% of chromium is reached. With respect to nickel, non-cold-worked material did not show differences between ductile and intergranular areas, being the average value around 9.5%.

Conditions with 10% cold work, named B, also showed phosphorus enrichment at grain boundaries, but with different levels depending on the heat treatment. At 500°C, 100 h, (B1), phosphorus level was as high as 3% while at 500°C, 1000 h, (B2), phosphorus average value

Table 5
Average atomic concentration calculated from Auger spectra

		A1	A2	A3	B1	B2	B3	C1	C2	C3
P	D	<0.1[a]	<0.1[a]	<0.1[a]	<0.1[a]	<0.1[a]	<0.1[a]	<0.1[a]	<0.1[a]	<0.1[a]
	IG	1.8 ± 0.9	1.8 ± 0.4	1.8 ± 0.7	3 ± 1	2.1 ± 0.8	1.0 ± 0.2	2.3 ± 0.2	3 ± 1	1.6 ± 0.6
Cr	D	19.5 ± 0.7	19.00 ± 0.01	19.2 ± 0.6	19 ± 1	18 ± 4	19 ± 1	17.8 ± 0.8	18 ± 1	19.4 ± 0.5
	IG	23 ± 4	23 ± 3	24 ± 5	28 ± 8	18 ± 3	23 ± 3	23 ± 3	19 ± 2	25 ± 4
Ni	D	10.0 ± 0.8	9.4 ± 0.6	9 ± 1	10 ± 1	10 ± 1	9.8 ± 0.9	12 ± 1	11 ± 2	12 ± 2
	IG	10 ± 2	9.1 ± 0.5	9 ± 1	8 ± 2	11 ± 3	9.4 ± 0.9	13 ± 2	13 ± 2	16 ± 2
Mo	D	ND[b]	ND[b]	ND[b]	ND[b]	ND[b]	ND[b]	ND[b]	ND[b]	ND[b]
	IG	1.6 ± 0.5	ND[b]	1.8 ± 0.4	1.5 ± 0.3	ND[b]	ND[b]	1.6 ± 0.5	1.58 ± 0.05	1.3 ± 0.2

[a] 0.1% is the Phosphorus detection limit of the AES.
[b] Molybdenum was not detected (ND) on these areas. Molybdenum detection limit was not found on consulted bibliography. As molybdenum concentration in matrix is 0.39 wt%, and that quantity has not been detected, it can be considered that AES detection limit for molybdenum is higher than this value.

was 2.1%. At 400°C, 1000 h, (B3), phosphorus has a similar level than in non-cold-worked condition, around 1%. It is worth noting that this condition presented a very small percentage of intergranular fracture, and the average value was calculated only over four data. Regarding chromium, condition B1 and B3 showed chromium enrichment, being higher in B1, 28% in average (reaching in some cases values higher than 30%), than in B3, 23%, the same as in non-cold-worked condition. On the other hand, condition B2 showed the same level as in ductile area, around 18%. With respect to nickel, B1 showed nickel depletion at grain boundaries with 8%, in average, compared to 10% at the ductile area, though some analyses at the intergranular area showed nickel higher than in the ductile area. In condition B2, the nickel average at intergranular area is 11%, which is similar to ductile area, though at some intergranular areas a 19% is reached. Condition B3 shows no difference between ductile and intergranular areas, as happened in non-cold-worked condition.

Finally, conditions with 30% of cold work, at 500°C, 100 and 1000 h, (C1 and C2) showed a phosphorus average value of 2.3% and 3%, respectively, while at 400°C, 1000 h, (C3), the phosphorus level is still similar to non-cold-worked condition, about 1.6%. On the other hand, condition C2 showed the same chromium level in ductile and intergranular areas, about 19%, while C1 and C3 showed chromium enrichment at intergranular areas, 23% and 25% respectively, similar to non-cold-worked condition. It is worth noting that analyses showing chromium depletion at grain boundaries were not found. Regarding nickel, enrichment is observed at intergranular areas in C2 and C3 conditions, with higher nickel in C3, 16%, than in C2, 13%.

Molybdenum was not observed in ductile areas, it was observed only in analyses on intergranular areas, but as has been explained before, not all analyses nor all conditions showed molybdenum. Average values where it appears were about 1.5%. It is worth noting that in all cases molybdenum appears joined with phosphorus and chromium peaks higher than in analyses without molybdenum.

Carbon and oxygen were observed to be present in all analyses for all conditions. Carbon concentration varied from 7% to 13% and oxygen from 11% to 19%, both at ductile and intergranular areas. Their origin is attributed to residual contamination from the vacuum chamber. It has been checked that the presence of these elements did not affect the relative concentrations of the rest of the elements.

3.3. Corrosion test results

Weight loss rate due to the $HNO_3 + Cr^{6+}$ corrosion test is recorded in Table 6 for every condition. It can be observed that the highest weight loss occurred for heat

Table 6
Average value of weight loss rate for each condition studied

Material condition	Weight loss rate (mg/cm^2 h)
A1	1.9 ± 0.2
A2	3.32 ± 0.04
A3	2.4 ± 0.1
B1	1.84 ± 0.08
B2	3.2 ± 0.4
B3	2.2 ± 0.1
C1	2.1 ± 0.3
C2	3.8 ± 0.3
C3	1.8 ± 0.1

treatment named 2, 500°C, 1000 h, for every cold work degree. It was observed that weight loss increased when temperature and duration of the heat treatment increased. A significant effect of cold work on this test was not observed.

On the other hand, the constant extension rate tests did not result in brittle fracture, nor intergranular not transgranular, being completely ductile in all conditions.

4. Discussion

The aim of the present work is to simulate particle irradiation effect by cold work followed by heat treatment. Under irradiation, there are two fundamental changes that take place in alloys: alteration of the structure and alteration of the chemical homogeneity, both developing simultaneously under irradiation at certain ranges of temperature. Structural changes at light water reactor temperature range involve the physical rearrangement of the lattice including formation and development of black spots, faulted dislocation loops and dislocation lines. Changes of the chemical homogeneity are manifested in local changes in the composition at free surfaces and grain boundaries. These changes in microchemistry are those we are concerned with in the present work.

During neutron irradiation, a non-equilibrium segregation could be induced at low temperatures that causes element concentration redistribution at grain boundaries and free surfaces. Point defects (interstitials and vacancies) are created by irradiation, reaching concentrations higher than in thermal equilibrium, leading to a net flow of defects towards sinks as grain boundaries, to annihilate [7]. Solute transport takes place when impurity or alloying atoms couple to point defect flow. Segregation towards grain boundaries resulting in element enrichment is driven by a preferential association with interstitials, while segregation away from grain boundaries leading to element depletion is driven by vacancy flux. On the other hand, several authors [8] explained that the sense of the segregation during irradiation seems to be related with an element factor size, if negative the segregation is towards interfaces and otherwise if positive. These results suggest that undersized substitutional atoms, as phosphorus, migrate towards grain boundaries and interfaces preferentially coupled with interstitial flow, while oversized elements travel preferentially with vacancy flow. Also, faster diffusing elements change places with vacancies flowing to sinks more frequently than slower diffusing species. Then, fast diffusing elements become depleted at sinks while slow diffusing elements are enriched. Taking in account all those mechanisms, regarding austenitic stainless steels, the resulting microchemistry at grain boundaries and interfaces by effect of irradiation in light water reactor conditions, could be phosphorus and nickel enrichment, and molybdenum, chromium and iron depletion [9]. This particular microchemistry has been related with material behaviour, being a factor to be considered as an IASCC cause.

As it has been explained in previous sections, in this work, microchemistry characterization by AES, in 304L cold worked and heat treated, shows phosphorus enrichment at interfaces in all studied conditions. Regarding other elements, chromium, molybdenum and nickel enrichment has also been observed in some cases. It is worth pointing out that chromium depletion at interfaces has not been observed.

Differences observed in microchemistry for different material conditions can be attributed to several possible factors. First at all, the initial characteristics of the material, regarding its microstructure and microchemistry have to be considered. As it has been shown in Section 3.1, initial microstructure consisted in delta-ferrite phase in an austenitic matrix. That initial state is determined by diffusion processes that take place during solidification when the material is manufactured. Cooling from high temperatures causes the redistribution of main alloying elements of the 304L of low carbon content, resulting in the formation of a delta-ferrite phase in an austenitic matrix which has a higher chromium content than the austenite phase and a lower nickel content. Also, through the cooling process, diffusion mechanisms provide chromium enrichment at the interface ferrite/austenite [10]. According to this author, phosphorus or molybdenum enrichment could also be present at that interface. These diffusion mechanisms involve non-equilibrium segregation of several components of the alloy that cause chromium and molybdenum diffusion to grain boundaries [11]. This initial microstructure and microchemistry will determine the existing microchemistry at those interfaces under the effect of subsequent processes, as cold work and heat treatments considered in the present study.

As has been said before, two types of spectra were obtained by AES. According to the above explanations, those which presented molybdenum, with high phosphorus and high chromium could be ferrite/austenite

interfaces, and the rest of the interfaces analysed were austenite grain boundaries. Almost all conditions showed both types of spectra, indicating that ferrite did not disappear with cold work or heat treatment. This fact agrees with microstructure observations already explained.

Conditions named A, with no cold work followed by heat treatments, show the same concentration levels of detected elements in spite of the three different heat treatments received. It is worth pointing out that these heat treatments are low enough to avoid significant changes in microchemistry. According to some authors [12], low phosphorus segregation is observed for heat treatments under 500°C, being the maximum segregation at 600–650°C in the case of a 304L. Also, it is known that these thermal treatments are too low to produce sensitization of this low carbon stainless steel. Furthermore, as it was previously mentioned, the material showed slight intergranular precipitation at 500°C, 1000 h and it did not show intergranular precipitation in the other two conditions (500°C, 100 h and 400°C, 1000 h). In addition, some Auger depth profiles performed at 500°C, 1000 h indicated that the thickness of the zone with chromium enrichment was too small to be attributed to precipitates. Then, the observed phosphorus and chromium enrichment, and also molybdenum presence in some cases, in these conditions are assumed to be due to elements redistribution by non-equilibrium segregation during cooling from high temperatures in fabrication processes and not to the thermal treatments.

Next, results from conditions B and C, that consisted of material with 10% and 30% of cold work, respectively, are discussed comparing them with results from non-cold-worked conditions named A.

Fig. 7(a)–(c) shows phosphorus concentration versus cold work degree. Fig. 7(a), corresponding to 500°C, 100 h, shows that B1 and C1 show an increase of phosphorus concentration compared to A1, being higher in B1 than in C1. Fig. 7(b), corresponding to 500°C, 1000 h, clearly shows that phosphorus concentration at grain boundaries increases when cold work degree increases. On the other hand, phosphorus does not show significant changes for different cold work degrees at 400°C, 1000 h as shown in Fig. 7(c). Briefly, it is observed that phosphorus concentration increased with cold work for 500°C, 100 and 1000 h, compared to non-cold-worked conditions A1 and A2. This fact is due to a non-equilibrium segregation process. When material has been cold worked, its vacancy and dislocation density is much higher that in equilibrium and when a heat treatment is applied, non-equilibrium segregation would be very fast [13]. The defects created by cold work could act as fast diffusion paths activated when temperature is applied, contributing to increase the segregation rate [14]. As the temperature of utilized heat treatments is too low to produce thermal segregation (500°C, 100 and 1000 h) it

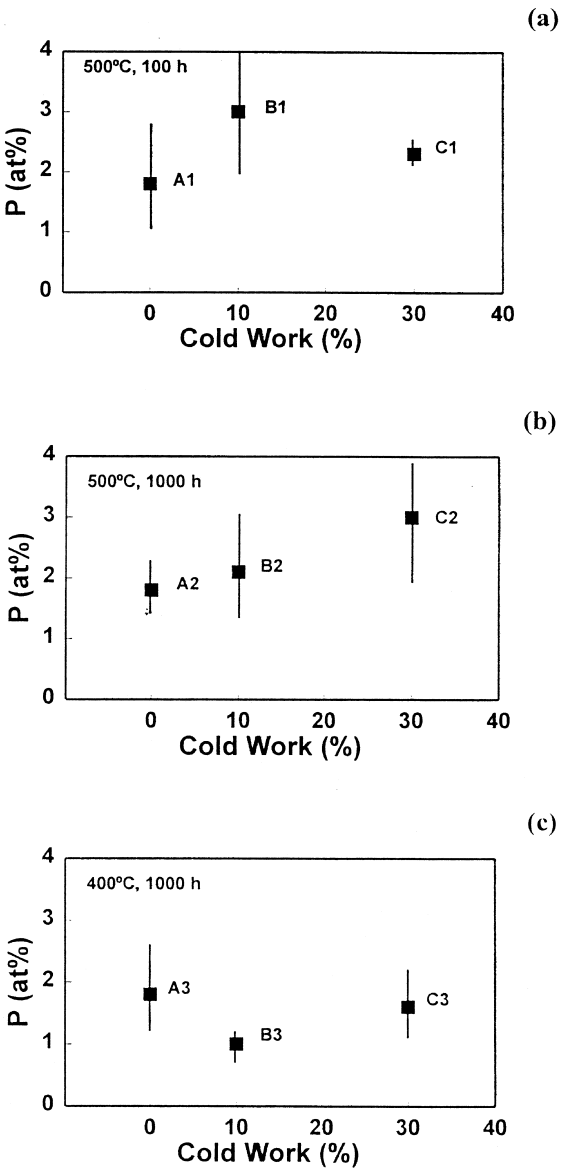

Fig. 7. Influence of cold work on phosphorus concentration at grain boundaries. (a) 500°C, 100 h, (b) 500°C, 1000 h, and (c) 400°C, 1000 h.

is cold work which helps and accelerates the process, giving place to phosphorus segregation at low temperatures. Results presented show that, qualitatively, the trend of phosphorus diffusion observed is similar to that observed by irradiation effect, for 10% and 30% of cold work at 500°C, 100 and 1000 h.

Regarding conditions B3 and C3 (10% and 30% of cold work, respectively, followed by a heat treatment of 400°C, 1000 h) where no significant change was observed compared to non-cold-worked condition A3, it

seems that 400°C is not high enough to allow created defect mobility. Then diffusion paths are not activated in this condition and no phosphorus segregation is observed that could be attributed to cold work.

Fig. 8(a)–(c) shows chromium concentration at interfaces versus cold work degree. In Fig. 8(a) for 500°C, 100 h, it is observed that condition B1 shows a higher chromium enrichment (28%) than non-cold-worked condition, A1, while C1 shows a similar level than A1 (~23%). It is worth mentioning that intergranular precipitation was not observed in these three conditions. As it is pointed by Seah [15], when chromium content is higher than necessary to make use of all carbon, the extra chromium may couple with phosphorus giving place to an interface enrichment, while if there were lower chromium, or more carbon, it is not so. This effect could be the cause of high chromium enrichment, joined to phosphorus enrichment in B1, both enhanced by cold work because condition A1, with no cold work, did not show such a high enrichment. On the other hand, conditions at 500°C, 1000 h with 10% and 30% of cold work, respectively, show neither enrichment nor depletion at interfaces compared to the matrix, about 19%. In this case, initial chromium pre-enrichment at interfaces prevents chromium depletion under the matrix concentration. However, the average chromium concentration (19%) implies a depletion compared to non-cold-worked condition A2 (23%), as can be observed in Fig. 8(b). In this sense, this depletion produced by a non equilibrium segregation away from grain boundaries, enhanced by cold work, is similar to the trend observed by radiation-induced segregation. Finally, conditions B3 and C3 show the same chromium level as A3, around 23%. Then, it is assumed that this heat treatment, 400°C, 1000 h, is not high enough to affect chromium diffusion.

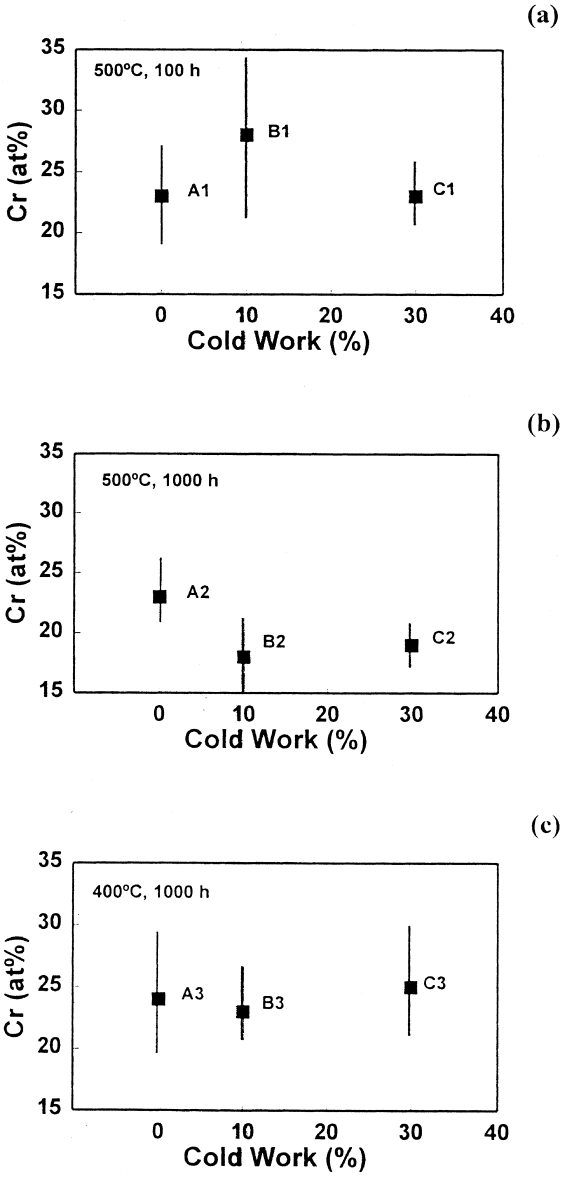

Fig. 8. Influence of cold work on chromium concentration at grain boundaries. (a) 500°C, 100 h, (b) 500°C, 1000 h, and (c) 400°C, 1000 h.

Anyway, cold work influence on chromium at interfaces seems to be quite complicated in the material studied because it has to take into account different processes other than segregation, which can interfere in the diffusion processes. As shown by metallography, in conditions with cold work, martensite formation at slips bands was observed, leading to transgranular carbide precipitation after the thermal treatment. Also, some intergranular precipitation was produced in conditions B2 and C2 (10% and 30% of cold work followed by 500°C, 1000 h). Then, in addition to non equilibrium segregation induced by cold work followed by heat treatment, chromium composition at interfaces could also be influenced by precipitation towards grain boundaries or slip bands. TEM/EDS studies are in progress to help the understanding of these phenomena.

In respect with other elements, no significant change in molybdenum concentration that could be attributed to cold work was observed. It is worth pointing out that non-equilibrium segregation induced by cold work also produced some nickel enrichment in conditions with the heat treatment at 500°C, 1000 h (B2 and C2).

As a summary of the above results, it can be said that cold work enhances phosphorus segregation towards interfaces at 500°C, 100 and 1000 h. On the other hand, chromium diffusion towards interfaces is enhanced at 500°C, 100 h and away from interfaces at 500°C, 1000 h. The heat treatment at 400°C, 1000 h seems to have no effect in spite of cold work. In consulted bibliography, [2,6,11,16–20], where the effect of irradiation with different particles is studied on similar materials, 304,

304L, 316, the trend observed is chromium depletion, and nickel and phosphorus enrichment, with different values depending on irradiation conditions and bulk concentrations. Regarding qualitative irradiation effect on segregation, the conditions used in the present work that seem to reproduce the same trend are those with 10% and 30% of cold work followed by 500°C, 1000 h. Quantitative comparisons are difficult due to pre-existing phosphorus and chromium enrichment. Then, regarding segregation to interfaces, cold work could be a good way to simulate irradiation effect.

Finally, we want to use segregation data to interpret HNO_3^+/Cr^{6+} corrosion test results. This test has been widely used to detect susceptibility to intergranular corrosion due to grain boundary impurities. We tried to correlate corrosion tests results with phosphorus presence at grain boundaries. Fig. 9 shows weight loss rate produced in this test versus phosphorus average concentration on grain boundaries measured by AES. In this graph, it is not possible to see a clear correlation between these two variables. In some cases, two material conditions with the same phosphorus average concentration showed different weight loss rates. The inhomogeneous distribution of phosphorus on the different interfaces could result in different weight loss even if the average values are similar. Also, the possible interactions between phosphorus and other alloying elements, as chromium, nickel and molybdenum, enriched at grain boundaries in some cases, could affect the ability of phosphorus to produce corrosion in this test [21].

It is worth pointing out that this test is able to detect other features present in the material, for instance chromium depletion to a level under 13%. As has been said before, none of the interfaces studied by AES showed such a low chromium concentration at interfaces. Heat treatments used were low enough to avoid sensitisation in this low carbon content material, and, on the other hand, the pre-existing chromium enrichment avoids a big depletion caused by non-equilibrium segregation. Therefore, weight loss cannot be attributed to sensitisation. According to Briant [21], steels containing martensite can have carbide precipitation at martensite layers, giving chromium depletion and therefore transgranular corrosion. Transgranular carbide precipitation at martensite layers has been observed in samples at 500°C, independently of the time of the heat treatment, and slightly at 400°C, and that, joined to the presence of residual delta-ferrite could be the reason for detected weight loss. All those variables present show that further work is needed to discern how the different factors involved can affect the corrosion properties of the AISI-304L stainless steel.

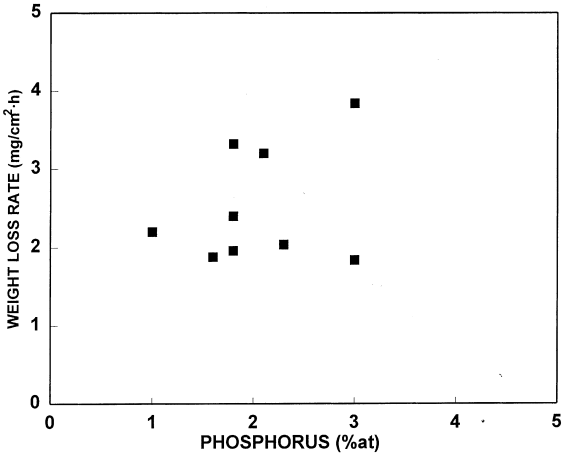

Fig. 9. Weight loss rate in the $HNO_3 + Cr^{6+}$ test vs. Phosphorus concentration at grain boundaries measured by Auger electron spectroscopy.

Regarding stress corrosion cracking susceptibility, the CERT results showed a completely ductile fracture. It seems that higher electrochemical potentials are needed as phosphorus promotes IGSCC in this test as shown in Jacobs studies [22], where a similar material was tested. There, cold work plus an anodic potential were required to produce some percentage of IGSCC.

5. Conclusions

Microchemistry at interfaces has been studied by AES on an austenitic stainless steel of type AISI-304L. The material was cold worked and then heat treated in order to simulate changes in microchemistry produced by neutron irradiation. The main results obtained in this study are the following.

- Two types of Auger spectra were obtained at interfaces. One type showed phosphorus enrichment while the other showed higher phosphorus enrichment associated to the presence of molybdenum and high chromium. The last ones have been attributed to ferrite/austenite interfaces, and the other to austenite grain boundaries.
- The heat treatments performed did not influence interface concentration on their own in non-cold-worked condition. Therefore, observed changes in phosphorus and chromium concentration at 500°C, 100 and 1000 h were attributed to cold work influence. Cold work enhanced non-equilibrium phosphorus segregation to interfaces and helped chromium diffusion away from interfaces, which did not result in chromium depletion due to pre-existing chromium enrichment.
- Results show that changes in microchemistry at grain boundaries in an austenitic stainless steel of type 304L, could be induced by cold work followed by heat treatments. The trends observed are similar to those observed when these steels are irradiated at

light water reactor temperature range. In this respect, regarding segregation to grain boundaries, cold work together with appropriate heat treatments, could be considered as a good way to simulate irradiation effect, as well as a useful help to understand its consequences in materials performance.

References

[1] P.L. Andresen, F.P. Ford, S.M. Murphy, J.M. Perks, in: Proceedings of the Fourth International Conference on Environmental Degradation of Materials in Nuclear Power Systems – Water Reactors, Jekyll Island, GA, August 1989, NACE, Houston.
[2] G.S. Was, S.M. Bruemmer, J. Nucl. Mater. 216 (1994) 326.
[3] L.E. Davis, N.C. MacDonald, P.W. Palmberg, G.E. Riach, R.E. Weber, Handbook of Auger Electron Spectroscopy, Physical Electronics Industries, Eden Prairie, MN, 1976.
[4] J.S. Armijo, Corrosion 24 (1968) 24.
[5] C.L. Briant, Corrosion 38 (1982) 230.
[6] S. Nakahigashi, M. Kodama, K. Fukuya, S. Nishimura, S. Yamamoto, K. Saito, T. Saito, J. Nucl. Mater. 179–181 (1991) 1061.
[7] P.R. Okamoto, H. Wiedersich, J. Nucl. Mater. 53 (1974) 336.
[8] K. Nakata, I. Masaoka, J. Nucl. Mater. 150 (1987) 186.
[9] J. Kameda, T.E. Bloomer, A.H. Swanson, D.Y. Lyu, J. Nucl. Mater. 252 (1998) 1.
[10] K. Easterling, Introduction to the Physical Metallurgy of Welding, Butterworth–Heinemann, London, 1992, p. 97.
[11] H.M. Chung, W.E. Ruther, J.E. Sanecki, A. Hins, N.J. Zaluzec, T.F. Kassner, J. Nucl. Mater. 239 (1996) 61.
[12] C.L. Briant, P.L. Andresen, Metall. Trans. A 19 (1988) 495.
[13] R. Chèron, X. Quillard, J.M. Roland, D. Roptin, Scripta Metall. Mater. 31 (1994) 423.
[14] A.V. Krajnikov, M. Militzer, J. Wieting, Mater. Sci. Technol. 13 (1997) 877.
[15] M.P. Seah, Acta Metall. 25 (1977) 345.
[16] E.A. Kenik, J. Nucl. Mater. 187 (1992) 239.
[17] D.L. Damcott, T.R. Allen, G.S. Was, J. Nucl. Mater. 225 (1995) 97.
[18] K. Nakata, I. Masaoka, J. Nucl. Mater. 150 (1987) 186.
[19] T.R. Allen, J.T. Busby, G.S. Was, E.A. Kenik, J. Nucl. Mater. 255 (1998) 44.
[20] W.J. Liu, J.J. Kai, C.H. Tsai, J. Nucl. Mater. 212–215 (1994) 476.
[21] C.L. Briant, A.M. Ritter, Metall. Trans. A 12 (1981) 910.
[22] A.J. Jacobs, Corrosion 46 (1990) 30.